Druck: Offsetschnelldruck
dbv-Verlag für die Technische Universität Graz
Uhlandgasse 8, 8010 Graz, Tel. 82-51-66

IIG – Report-Series

IIG: Institutes for Information Processing Graz[1]

Comparison of Different Light Reflection Models

K.F. Karner, E.A. Deutschl, F.W. Leberl

Report
399
November 1994

[1]The IIG are a group of research institutes cooperating under the auspices of the Austrian Computer Society OCG (Division Graz) in a variety of matters, including this series of reports. The IIG currently include twelve institutes as follows: (a) Applied Information Processing and Communications Technology, (b) Applied Mathematics and Computer Science, (c) Computer Graphics and Computer Supported Geometry (d) Information Processing and Computer Supported New Media, (e) Information Science, (f) Information Systems, (g) Medical Informatics I, (h) Medical Informatics and Neuroinformatics, (i) Multi-Media Information Systems, (j) Software Technology, (k) Technical Informatics, and (alphabetically last but not least) (l) Theoretical Computer Science.

Comparison of Different Light Reflection Models

Konrad F. Karner, Edwin A. Deutschl, Franz W. Leberl

Institute for Computer Graphics
Graz University of Technology
Münzgrabenstraße 11
8010 Graz
Tel.: +43 (316) 84 17 66-22
Fax: +43 (316) 84 63 04
e-mail: karner@icg.tu-graz.ac.at

Abstract

"Photo-realism" in 3-D rendering requires the use of mathematical models of light reflection which optimally approximate the physical reality. We are therefore interested in an understanding of the limitations of commonly used light reflection models. We compare different algorithms to calculate the bidirectional reflection distribution function (BRDF), and relate the results to physical measurements. We focuse our study to quantify the differences among calculated BRDF's, and between such BRDF's and physical measurements. We also concern ourselves with issues of computing resources.
We consider algorithms based on empirical models and on physically based models where the need exists to exactly describe a material's properties. The error of a simulation is obtained from a comparison with measured data. We find that none of the models produce good results consistently with all measurements, but with carefully calibrated parameters the errors could be reduced for some materials to less than 3%.

1 Introduction

Recent years have witnessed great efforts to improve the quality of global illumination algorithms for use in photorealistic rendering applications. To achieve photorealism we need to understand the requirements which the input data for those illumination models must satisfy, and we must concern ourselves with rigorous reflection models for different materials on 3-D objects to be rendered.

In this paper we investigate different reflection models, ranging from empirical models to rigorous physically based models. One important condition for the validity of global illumination algorithms like radiosity is the so-called "energy equilibrium". For instance, the very frequently used Phong model [Phong,1975] violates this requirement and fails to secure energy consistence. In addition there is no connection with a given material's properties such as surface roughness, refraction index and so on, while these are necessary elements for the simulation of different surfaces and types of reflection. To establish such a link requires that physically based reflection models should be used for global illumination.

Such models need parameters to describe surface material properties. We demonstrate the measurement of such properties in the laboratory, and quantify the ability of certain reflection algorithms to actually model a given material's known appearance.

2 Bidirectional Reflectance Distribution Function

The reflection of light on a surface is oftentimes described by a so-called bidirectional reflectance distribution function BRDF. This is the relationship between reflected radiance I_r and the incident irradiance I_i from direction ω_i(see Equation (1) and (2))*.

$$I_r = \int_{\omega_i \in \Omega} \rho_{bd} I_i (\boldsymbol{N} \bullet \boldsymbol{L}) d\omega_i \qquad (1)$$

$$\rho_{bd} = \frac{dI_r}{I_i \cdot (\boldsymbol{N} \bullet \boldsymbol{L}) \cdot d\omega_i} \qquad (2)$$

Figure 1 defines various geometric elements of equation (1) and (2) and Table 1 explains its various parameters.

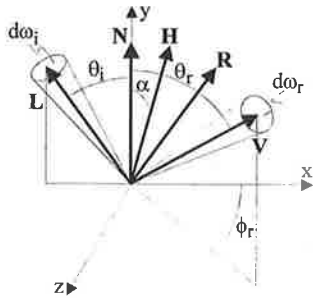

Figure 1: Relationship between reflected radiance I_r and irradiance I_i

Normally the BRDF is shown in polar coordinates. The polar angle represents the reflection angle θ_r. The value of the BRDF is given by the polar radius which is normalized in reflection direction. We will use such diagrams to present the results of certain light reflection models and of actual physical measurements.

3 Different Light Reflection Models

Our desire to achieve photorealism has led to the study of the properties of several commonly used reflection models. To develop a thorough understanding about these models we developed a software library containing some classical as well as some recently published models. These are fairly complex to derive; therefore we abstain from a review of such derivations but refer to the original publications where such derivations can be studied.

* Annotation: The vectors **N,L,V,R,H** are unit vectors. The symbol " • " denotes a vector in-product.

N	surface normal vector
L	light vector (incident direction)
$d\omega_i$	solid angle, placed around the light vector
I_r	reflected radiance
dI_r	reflected radiance in one direction
ρ_{db}	bidirectional reflectance distribution function (BRDF)
Ω	hemisphere arround N
V	view vector (reflectance direction)
$d\omega_r$	solid angle, placed around the view vector direction
R	reflection vector (reflectance direction) ($2(\boldsymbol{N} \bullet \boldsymbol{L})\boldsymbol{N} - \boldsymbol{L}$)
H	bisector vector between **L** and **V**
F	Fresnel factor
G	geometrical attenuation factor
D	microfacet distribution function
α	angle between **N** and **H**
m	rms slope of the microfacets
g	apparent roughness
σ_h	root mean square (rms) roughness
τ	correlation distance
ϕ_r	deviation angle between reflection plane and view vector **V**
λ	wave length
dA_s	infinitesimal surface area
Δ	Dirac-function

Table 1: Parameters used in the BRDF and light reflection models.

3.1 Empirical Models

Phong-Blinn

The Phong model was first defined in [Phong, 1975]. It's BRDF is:

$$\rho_{bd} = k_d + k_s \frac{F_s}{(\boldsymbol{N} \bullet \boldsymbol{L})} \qquad (3)$$

with $$F_s = (\boldsymbol{R} \bullet \boldsymbol{V})^{N_P} \qquad (4)$$

The factor F_S was changed by Blinn [Blinn, 1977] in the following way:

$$F_s = (\boldsymbol{N} \bullet \boldsymbol{H})^{N_B} \qquad (5)$$

The properties of a given surface material are characterized by parameters k_d as the fraction of light diffusely reflected, k_S as the fraction specularly reflected, N_P and N_B as an index that controls the "tightness" of specular highlight.
It is generally understood that this model produces good results, for example in the visualization of plastic materials and provided that the parameters k_d, k_S, N_P and N_B are carefully chosen. However, this model lacks a link into physical parameters of a material and it fails to preserve energy consistence [Lewis,1993]. Blinn's modification approximates Phong's model and achieves a faster calculation.

3.2 Geometrical Optics Models

Torrance-Sparrow

Torrance and Sparrow (1967) introduced a category of models for rough surfaces only. This is defined by:

$$\rho_{bd} = \frac{FGD}{\pi(N \bullet L)(N \bullet V)} \tag{6}$$

Modifications of this model are possible through an exchange of methods to calculate the terms F (Fresnel factor), G (geometrical attenuation factor) and D (distribution function). For instance, because it achieves great simplification and only small differences, Schlick (1992) computes this geometrical attenuation factor G by:

$$G = G(v) \cdot G(v') \tag{7}$$

$$G(v) = \frac{v}{r - rv + v} \qquad G(v') = \frac{v'}{r - rv' + v'} \tag{8}$$

where $v = (\mathbf{V} \bullet \mathbf{N}) \qquad v' = (\mathbf{L} \bullet \mathbf{N})$ (9)

and r ($\in [0, 1]$) is a parameter of surface roughness.

If the surface is approximated by small, ideally smooth facets (microfacets), then the microfacet distribution function D interprets the probability of microfacets which contribute to the reflection from **L** to **V**. It must be considered a disadvantage of most distribution functions that the user needs to choose certain parameters. Cook-Torrance (1982) therefore defined a distribution function D for the Torrance-Sparrow model without chooseable parameters:

$$D = \frac{1}{4m^2 \cos^4 \alpha} e^{-\frac{\tan^2 \alpha}{m^2}} \tag{10}$$

Schlick

Schlick (1993) presents an approximation of the model by Torrance-Sparrow and Cook-Torrance with rational functions. This model provides energy consistence and handles anisotropic reflection. The BRDF is defined by the product of a spectral factor F_λ and direction factor D:

$$\rho_{bd} = F_\lambda(u) D(t, v, v', w) \tag{11}$$

$$t = (\mathbf{H} \bullet \mathbf{N}) \quad u = (\mathbf{V} \bullet \mathbf{H}) \quad v = (\mathbf{V} \bullet \mathbf{N}) \quad v' = (\mathbf{L} \bullet \mathbf{N}) \quad w = \cos \phi_r \tag{12}$$

$$F_\lambda(u) = F_0 + (1 - F_0)(1 - u)^5 \tag{13}$$

F_0 ($\in [0,1]$) represents the Fresnel factor with an incident angle of 0° and given wavelength. r ($\in [0,1]$) is called surface roughness factor. It relates to the rms slope m of the microfacets as follows:

$$r = \sqrt{\frac{2}{\pi}} m \tag{14}$$

p ($\in [0,1]$) is called the "isotropic factor"; p=1 is perfect isotropy, p=0 is anisotropy. It is defined by the proportion of the rms slope in brush direction to the rms slope normal to brush direction.
The direction factor D can be defined in several ways. The most flexible is the following:

$$D(t, v, v', w) = \frac{1 - G(v)G(v')}{\pi} A(w) + \frac{G(v)G(v')}{4\pi v v'} Z(t) A(w) \tag{15}$$

It accounts for self shadowing and reemission.
Z(t) represents the dependence of the direction factor D on zenith angle α and A(w) the dependence on azimuth angle ϕ_r:

$$Z(t) = \frac{r}{\left(1 + rt^2 - t^2\right)^2} \tag{16}$$

$$A(w) = \sqrt{\frac{p}{\left(p^2 - p^2 w + w^2\right)}} \tag{17}$$

Z(t) and A(w) have the shape of an ellipse. For instance if r=1 (that means a rough surface) Z(t) equals a circle. As r approaches 0 (smooth surface), Z(t) will be represented by an ellipse with very high eccentricity. The same properties are valid for A(w). These functions perform the requirements for reciprocity and energy consistence [Schlick,1993,pg80]. The shadowing function G is identical to that in the Torrance-Sparrow model.

The advantage of Schlick's model is its simplicity. Nevertheless there is no violation of physical restrictions and anisotropic reflections are handled easily.

3.3 Physical Optics Models

Beckmann-Spizzichino

Beckmann and Spizzichino (1967) based their model on the theory of electromagnetic waves. This model is valid under some restricted assumptions. The surface has to show certain properties, for instance it must be a conductive material. There are also some restrictions on the electromagnetic waves [Nayar et al.,1991,pg617].

$$\rho_{bd} = \frac{(N \bullet L)}{\lambda^2} e^{-g} \left(\frac{dA_S}{(N \bullet V)} \Delta + \frac{\pi \tau^2 D_g^2}{(N \bullet V)} \sum_{i=1}^{\infty} \frac{g^i}{i!\,i} e^{-\frac{v_{xz}^2 \tau^2}{4i}} \right) \tag{18}$$

with

$$g = \left(k \sigma_h ((N \bullet L) + (N \bullet V))\right)^2 \tag{19}$$

$$D_g = \frac{1 + \cos\theta_i \cos\theta_r - \sin\theta_i \sin\theta_r \cos\Phi_r}{\cos\theta_i (\cos\theta_i + \cos\theta_r)} \tag{20}$$

$$v_{xz} = \sqrt{v_x^2 + v_z^2} \tag{21}$$

$$k = \frac{2\pi}{\lambda} \tag{22}$$

$$v_x = k(-\sin\theta_i + \sin\theta_r \cos\phi_r); \quad v_y = k(\cos\theta_i + \cos\theta_r); \quad v_z = k(\sin\theta_r \sin\phi_r) \tag{23}$$

This model consists of two components. The first is the specular-spike component $f(e^{-g})\Delta$. Because of the dependence on wavelength it will be considered that a rough surface looks smooth for long-waved light and shows specular reflection. The specular-lobe component is distributed around the specular-spike component. It results from scattering of light because of surface roughness.
The distribution function consists of an infinite sum which results in an expensive calculation. Nayar et al. (1991) present two approximations for smooth (g<<1) and rough (g>>1) surfaces.

He-Torrance-Sillion-Greenberg

The He-Torrance-Sillion-Greenberg model [He et al.,1992] is also based on the theory of electromagnetic waves. Many different materials from conductive to nonconductive and from smooth to rough surfaces can be processed by this model:

$$\rho_{bd} = \rho_{bd,sp} + \rho_{bd,dd} + \rho_{bd,ud} \tag{24}$$

with

$$\rho_{bd,sp} = \frac{FGe^{-g}}{(\mathbf{N}\bullet\mathbf{L})d\omega_i}\Delta \tag{25}$$

$$\rho_{bd,dd} = \frac{FG}{(\mathbf{N}\bullet\mathbf{L})(\mathbf{N}\bullet\mathbf{V})}\frac{\tau^2}{16\pi}\sum_{i=1}^{\infty}\frac{g^i e^{-g}}{i!\,i}e^{-\frac{v_x^2\tau^2}{4i}} \tag{26}$$

$$\rho_{bd,ud} = a(\lambda) \tag{27}$$

Conductive and nonconductive materials are considered by the proportional relation between the Fresnel factor F and the specular term $\rho_{bd,sp}$. The effect of self shadowing and -masking is handled by the shadowing factor G. The decrease of the surface roughness results in refraction and interference effects, that means that the reflected light is scattered. This scattering has a preferred direction and is modeled by the second term $\rho_{bd,dd}$. The third term $\rho_{bd,ud}$ describes the diffuse effect which arises from multiple reflections.

3.4 General Models

Nayar

Physical models are able to calculate the reflection of surfaces, but their disadvantage lies in high calculation cost. Nayar et al.(1991) show that the direct diffuse term of the physical model from Beckmann-Spizzichino can be replaced by the reflection model of Torrance-Sparrow:

$$\rho_{bd} = \rho_{bd,sp} + \rho_{bd,dd} + \rho_{bd,ud} \tag{28}$$

with

$$\rho_{bd,sp} = \frac{(\mathbf{N}\bullet\mathbf{L})dA_s}{\lambda^2(\mathbf{N}\bullet\mathbf{V})}e^{-g}\Delta \tag{29}$$

$$\rho_{bd,dd} = \frac{kFG}{4(\mathbf{N}\bullet\mathbf{L})(\mathbf{N}\bullet\mathbf{V})}e^{-\frac{\alpha^2}{2\sigma_\alpha^2}} \tag{30}$$

$$\rho_{bd,ud} = C_{dl} \tag{31}$$

Thus the model is valid under general conditions, yet manages to execute at a decreased calculation expense.

One might build combinations of models. For example the model from Nayar could be augmented by the specular term of the He-Torrance model, the direct diffuse term from Torrance-Sparrow or from Cook-Torrance.

3.5 Overview

The most important elements of the six light reflection models are summarized in Table 2. Physical measurements on surface materials can be used in almost all of these methods.

Method	Energy Consistence	Parameter	Calculation expense
Phong-Blinn	no	empirical	minimum
Torrance-Sparrow-Cook	yes	partly measurable	relative small
Beckmann-Spizzichino	yes	measurable	high
Nayar	yes	measurable	smaller than Beckmann-Sp.
He-Torrance et al.	yes	measurable	high
Schlick	yes	measurable, and intuitive choice	small

Table 2: Summary of light reflection models for photorealistic rendering.

3.6 Sources of Input Data

Surface roughness is commonly described by the root mean square (rms) roughness σ_h of the normal distributed height of a surface and its autocorrelation distance τ. These parameters can be measured with a stylus type tactile roughness measurement system where a diamond tip is moved over the surface. The variation in the vertical position is measured and evaluated with a tolerance of ±5%. A disadvantage of this method is that many materials, for example textile or other soft materials, cannot be measured. In these cases one would need to employ optical methods which are more complex.

4 Measuring Light Reflection

Ideally we would like to be able to measure reflected light of an object in the field. However, this is commonly not feasible unless one were to develop a specialized measuring arrangement. Therefore common reflection measurements are being performed in a laboratory.

4.1 Experimental Setup

The BRDF can be measured by a photogoniometer. The configuration of a typical measuring instrument is shown in Figure 2. A specimen to be measured has to be small, with dimensions not exceeding 1 x 1 inches. This arrangement therefore lends itself to characterize only small fragments of objects which may occupy large spaces in the real world.

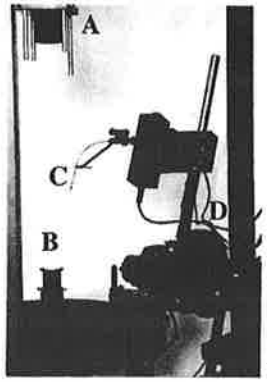

Figure 2: General view of the measuring system

The material under investigation is placed on table B. It is illuminated by a standardized and fixed light source, e.g. a halogen lamp 20W with integrated filtering. The movable light detector C measures the irradiance of the reflected light. This information is stored by a computer. During the measurement the light detector is moved over the material. To measure different ingoing direction **L** the material must be rotated with respect to the light source. Measurements are possible to a position of 15° under the horizontal plane of table B. The results of the measurement are available in ASCII-format.

4.2 Limitations of the Measurement

Measurements of the reflection direction **V** are feasible up to 90°, provided that the incidence angle θ_i is smaller than 15°. We collected measurements at two different angles θ_i=15° and θ_i=40°, so that the reflection direction **V** range is limited to 65° in the case where the incidence angle θ_i is 40°.
The error of measurements is proportional to the reflection angle. The average error is ±0.5%.

5 Computing Times of Different Reflection Models

The time to compute different models depends on the input data. So we used the same method as Schlick (1992) to evaluate the calculation time. The input parameters were varied randomly within their input range and the calculation was repeated 10^6 times to get a good range of parameters, e.g. from very smooth to very rough materials. Table 3 summarizes the results.

Light reflection model	Speed up	Speed up (with approx. sum)
He-Torrance	1	1
Beckmann-Spizzichino	1.1	2.9
Nayar	3.6	2.3
Torrance-Sparrow	5.7	3.7
Schlick	6.7	4.4

Table 3: Computing times of various light reflection models.

The values in Table 3 present the speed up against the model with the longest calculation time (He-Torrance). The last column considers that the infinite sums in the models of He-Torrance and Beckmann-Spizzichino can be approximated by simpler terms (chapter 3.2).

6 Comparison between Measured and Computed Reflection Data

We have initial results with three different materials. Quantitative results need to be based on a definition of errors. The error is defined as the area between calculated and measured BRDFs in the polar coordinate system, divided by the measured BRDF, as shown in Figure 3.

6.1 Chrome

Chrome confirms the expectation that it exhibits mainly specular reflections. The values for the refraction and extinction coefficients can be found in the literature, e.g. [Landolt et al.,1987]. Figure 3 presents different reflection models and their comparison with the measurements. The calculated data are shown as black solid lines, whereas the measurements are thin gray lines. In the event of a surface made of chrome, we will not see differences among the various reflection methods, nor vis-a-vis the measurements. Only in the case of the model by Schlick do we even begin to note visible differences.

We can quantify the errors to be in the range of approximately 40%. The reason for this relatively great errors is that in the calculation of the errors there is a division by the area of the measured BRDF which is very small in the case of specular reflection.
If the roughness factor r is changed towards 0, Schlick's model can be improved to an error of approximately 30% (see Figure 3.f).

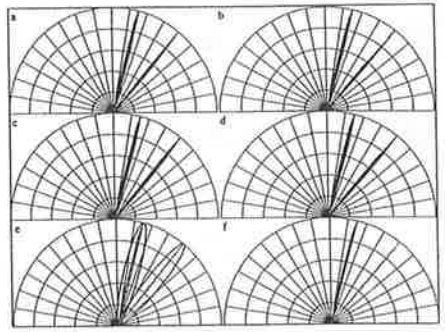

Figure 3: (a) He-Torrance, (b) Beckmann-Spizzichino, (c) Torrance-Sparrow, (d) Nayar, (e) Schlick, (f) Schlick with changed roughness factor r

6.2 Veneer

Veneer shows the full range of specular and diffuse reflections. We used veneer designated as "Fiume rough" and produced by a kitchen manufacturer (DAN Küchen) for use in indoor environments. The problem of such materials is that the refraction index n is unknown or, at least only known for a single wavelength. Characterization of such materials requires light reflection measurements. We approximate the refractive index n for this material: n=1.6 at λ=0.546 (green).

Figure 4.a presents the reflection model of He-Torrance with a roughness factor σ_h=3.05 and a correlation distance τ=40μm. The value of the diffuse term is 0.23. The error is 4.9%. By increasing the diffuse term to 0.265 (see Figure 4.b) without violating the energy consistence, the error reduces to less than 2.6%.
The Beckmann-Spizzichino model is defined for conductive materials only and is therefore not applicable here. Figure 4.c presents the Torrance-Sparrow model with an error of 22%. In figure 4.d the diffuse value is changed to reduce the error to 7.2%. Nayar's model (Figure 4.e) produces an error of 7% with a diffuse term of 0.23.
Finally the model of Schlick in Figure 4.f results in an error of 21%. The error can be reduced if the roughness factor r is increased lightly, but considerable differences with the measurements remain.

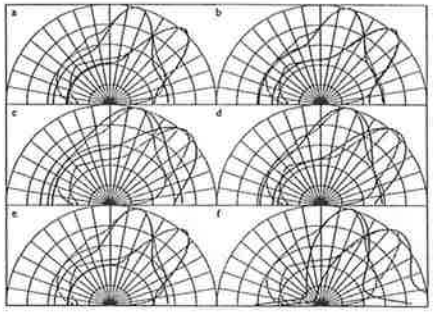

Figure 4: (a) He-Torrance, (b) He-Torrance with changed diffuse term, (c) Torrance-Sparrow, (d) Torrance-Sparrow with changed diffuse term, (e) Nayar, (f) Schlick

6.3 Paint

Wall-paint is generally very important when rendering indoor scenes. We therefore studied paint #D2109 (Distler); our sample was painted on a piece of paper. It features a rough surface and thus diffuse reflections. The surface roughness could not be measured with the tactile profiling method. Therefore we had to rely on "reverse engineering" by varying rendering parameters so that the result fit well with the measurements.

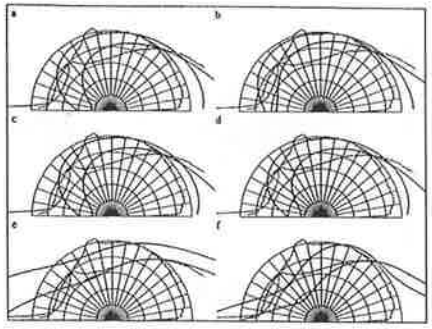

Figure 5: (a) He-Torrance, (b) He-Torrance with changed refraction index n, (c) Torrance-Sparrow, (d) Nayar, (e) Schlick, (f) Schlick with changed roughness factor r
Figure 5.a shows the He-Torrance model with a diffuse term of a(λ)=0.02 and an error of 14.6%. To reduce this error we must reduce the refraction index, as shown in Figure 5.b. The error of the models from Torrance-Sparrow and Nayar have the same value (see Figure 5.c, 5.d). Schlick's model (r=0.48) in Figure 5.e shows significant differences at an incidence angle of 15°. If the roughness factor r is decreased (r=0.3), then the total error is reduced, while the error at an incidence angle of 40° increases (Figure 5.f).

7 Visualization of three different types of reflection functions

In Figure 6 we visualized three different types of reflection functions. The left sphere and cylinder exhibit diffuse reflection. The middle ones show us a direct diffuse, and the right a specular reflection function. In addition the middle and right cylinder exhibit an anisotropic reflection function which was produced by the model from Schlick.

8 Conclusions and Future Work

We present initial results from measurements of certain materials for use in photorealistic rendering applications. A total of six methods to compute light reflections were employed and three distinctly different materials were used: chrome, veneer, paint.
Comparison between rendering methods and actual reflective properties are based on the area between two BRDF curves, divided by the area enclosed by the measured BRDF.

All reflection models except the approximation by Schlick deliver results, with errors less than 40% when specular reflection occures.

None of the reflection models produce good results consistently with all measurements. The smallest errors occur with the model by He-Torrance.

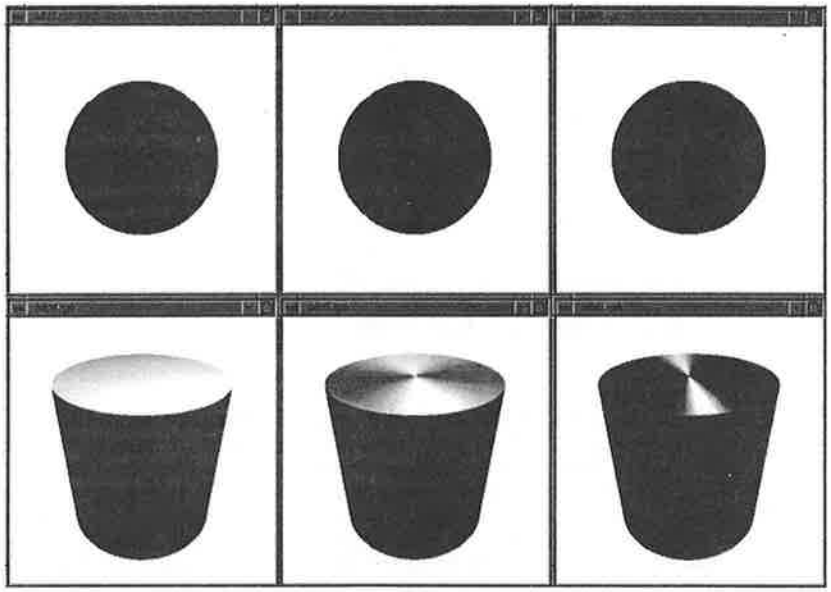

Figure 6: Visualization of three different types of BRDF's.

If computing speed is of concern, then the model by Nayar is of interest. It consists of three reflection terms and is applicable with only minor restrictions on surfaces. Relatively good results can be produced by varying the calculation terms of this model, e.g. the distribution function from Beckmann was used and Schlick's formulation of the shadowing function were used instead of the original shadowing function .

Schlick's model is fast. While its errors of the BRDF are consistently larger than in other models, but the characteristic still meets the measurements. The parameters can be choosen intuitively and anisotropic effects can be handled without additional calculation.

Many of the materials used in indoor scenes have reflective properties that are not known. We have demonstrated a technique to determine relevant data about various materials for use in different light reflection models. Such measurements are needed to avoid errors in rendering in the range of 30% or more.

The use of a photo-goniometer is straight forward, but requires a laboratory set-up. We find that it would be advantageous to use a field-device in existing environments to determine the required data for photorealistic rendering of extended and varied scenes.

References

Beckmann P., Spizzichino A.: The Scattering of Electromagnetic Waves from Rough Surfaces, Pergamon Press 1963.

Blinn, J. F.: Models of Light Reflection for Computer Synthesized Pictures, Computer Graphics, vol. 11, no. 2, July 1977.

Cook R. L., Torrance K. E.: A Reflectance Model for Computer Graphics, ACM Transactions on Graphics, vol. 1, no. 1, January 1982, pp. 7 - 24.

Deutschl E. A.: Implementierung und Vergleich verschiedener Modelle zur Berechnung von Reflexionsfaktoren, Diploma Thesis, University of Technology Graz, Austria, 1994.

He X. D., Torrance K. E., Sillion F. X., Greenberg D. P.: A Comprehensive Physical Model for Light Reflection, Computer Graphics, vol. 25, no. 4, July 1991 (SIGGRAPH '91), pp. 175 - 186.

Landolt, Boernstein: Zahlenwerte und Funktionen aus Naturwissenschaft und Technik, Neue Serie, Gruppe 3, Bd. 22, Springer 1987.

Lewis R. R.: Making Shaders More Physically Plausible, Fourth Eurographics Workshop on Rendering, Paris, France, June 1993, pp. 47 - 62.

Nayar S., Ikeuchi K., Kanade T.: Surface Reflection: Physical and Geometrical Perspectives, IEEE Transactions on Pattern Analysis and Machine Intelligence, vol. 13, no. 7, July 1991, pp. 611-634.

Phong B. T.: Illumination for Computer Generated Pictures, Communications of the ACM, vol. 18, no. 8, pp. 311-317, 1975.

Schlick C.: Divers éléments pour une synthèse d'images réalistes, PhD Thesis, Université Bordeaux 1, France, 1992..

Schlick C.: A Customizable Reflectance Model for Everyday Rendering, Fourth Eurographics Workshop on Rendering, Paris, France, June 1993, pp. 73 - 83.

Torrance K. E., Sparrow E. M.: Theory for Off-Specular Reflection from Roughned Surfaces, Journal of Optical Society of America, vol. 57, no. 9, 1967.

ONLY REPORTS PUBLISHED SINCE 1990 ARE LISTED:

278) Picture Interchange Coding (PIC); Addendum 1 - PIC Text Encoding, Addendum 2 - PIC Vtx Profile (K.Andrews, K.Rapatz)

279) The Viewseum - An Introduction (H.Maurer)

280) User modelling and database selection in information retrieval (S.Dominich)

281) Measuring the complexity of programs formed from actions (F.Huber)

282) Presentation metaphors for a very large hypermedia system (G.Davies, H.Maurer, J.Preece)

283) HOTACT: HOmeTrainer And Computer Technology (H.Maurer, G.Soral)

284) Hyper-G Specification of Requirements (Revised Version) (F.Kappe, H.Maurer, I.Tomek)

285) Animation in Hyper-G - An Outline (F.Kappe, H.Maurer)

286) Hypermedia Bibliography (H.Maurer, I.Tomek)

287) Factoring Cartesian-Product Graphs at Logarithmic Cost per Edge (F.Aurenhammer, J.Hagauer, W.Imrich)

288) Bounded Delay L Codes (H.Maurer, A.Salomaa, D.Wood)

289) A Transputer Based Lan Concept (R.Posch, F.Pucher, M.Welser)

290) Multiplication As Parallel As Possible (P.Lippitsch, K.C.Posch, R.Posch)

291) Security issues when implementing a hierarchical cluster of local area networks (R.Posch, P.Lipp)

292) CGI' Interface Version 1.0 (based on CGI 2nd DP) (W.D.Fellner, F.Kappe, J.Schäffler)

293) PC-RSA A cryptographic toolkit for MS-DOS (P.Lippitsch, R.Posch)

294) A Conceptual View of MS-DOS File System Security (R.Posch, M.Welser)

295) Computer Visualization, a Missing Organ, and Cyber-Equivalency (H.Maurer, P.Carlson)

296) BRAINDEX-G Computer-based Decision Support for Brain Death Diagnosis in Clinical Practice (R.Grims, G.Schwarz, E.Rumpl, G.Rom, G.Pfurtscheller)

297) Hypermedia Systems and Other Computer Support as Infrastructure for Museums (H.Maurer, M.Williams)

298) Sleep Stage Monitoring in Infants - Signal Recording, Data Processing and Preliminary Results (G.Pfurtscheller, G.Litscher)

299) BRAIN-COMPUTER INTERFACE: Prediction of Hand Movements from Single Trial Multi-Channel EEG Data with a Neural Network - Preliminary Results (G.Pfurtscheller, D.Flotzinger, W.Mohl)

300) The Institutes for Information Processing in Graz, Austria (IIG) (H.Maurer)

301) Electrophysiological Correlates of Cortical Areas During Information Processing and Idling (G.Pfurtscheller)

302) Integrated Diagnostic Imaging Digital PACS in Medicine 1980-2000 (G.Gell, M.Wiltgen)

303) Using a Transputer Cluster in a Classroom Environment (R.Posch, F.Pucher, M.Welser)

304) Cost-Benefit Analysis of Personal Computer Productivity: A Comparative Study between U.S. and a European (Austrian) Organization (Th.Weitzendorf, R.Wigand)

305) A Survey Study on Approaches in Technology Transfer, Software Management and Organization (V.Haase, R.Messnarz)

306) OPERAS: A rule-based expert system for error detection and elimination in a PACS (M.Wiltgen, G.Gell)

307) Transformation matrices of clock-controlled shift registers (D.Gollmann)

308) Aspects of a Modern Multi-Media Information System (F.Kappe)

309) Cost-Benefit Analysis on the Information-Gathering Regulated by the Paperwork Reduction Act 1980: Arguments for its Feasibility and a Reconsideration of the Burden Box Approach (Th.Weitzendorf, R.Wigand)

310) Sleep monitoring in human adults: Continuous monitoring of brainstem auditory evoked potentials and analysis of non-invasive blood pressure, heart rate - and respiratory parameters in all-night polysomnographics recordings (G.Litscher, E.Körner, G.Pfurtscheller)

311) A method for time domain analysis of EMG at higher levels of muscle contraction (E.Zens, G.Jöchtl, G.Rom, G.Pfurtscheller, E.Rumpl, Ch.Stadler)

312) A fast method for modulus reduction in Residue Number System (H.Hassler, O.Aichholzer)

313) Modulo arithmetic on parallel processors - a case study (R.Posch)

314) A Hierarchical View of Time (P.Gillard, K.C.Posch)

315) Links in Hypermedia Systems (H.Maurer, I.Tomek)

316) Algorithms and Lower Bounds for On-line Learning of Geometrical Concepts (W.Maass, G.Turan)

317) Improved Space for Bounded Space On-Line Bin-Packing (G.Wöginger)

318) Heuristics for Parallel Machine Scheduling with Delivery Times (G.Wöginger)

319) An On-Line Scheduling Heuristic with Better Worst Case Ratio than Graham's List Scheduling (G.Galambos, G.Wöginger)

320) Tasks and Decisions: A Suggested Model to Demonstrate Benefits of Information Technology (Th.Weitzendorf, R.Wigand)

321) How fast can a threshold gate learn? (W.Maass, G.Turan)

322) Lower bound methods and separation results for on-line learning models (W.Maass, G.Turan)

323) Neural Network Classification of Spatio-temporal EEG Patterns (N.Masic, G.Pfurtscheller)

324) Neural Network-based Classification of Spatiotemporal EEG-Data (D.Flotzinger)

325) Design for a fast arithmetic unit using RNS-Float-Reduction (R.Posch)

326) Exactly Approximated Base Extension in Residue Number Systems (K.C.Posch, R.Posch)

327) Modulo Reduction in Residue Number Systems (K.C.Posch)

328) Neural Network based Classification of Non-averaged Event-related EEG responses (M.Peltoranta, G.Pfurtscheller)

329) Computing the Optimum Stock Size (H.Kellerer, F.Rendl, G.Wöginger)

330) Angle-Restricted Tours in the Plane (S.Fekete, G.Wöginger)

331) Why Hypermedia Systems are Important (H.Maurer)

332) A Parallel Approach to Long Integer Register Oriented Arithmetic (R.Posch)

333) Hyper-G, A Universal Hypermedia System (F.Kappe, H.Maurer, N.Sherbakov)

334) A Highly Parallel Ciphering Concept (R.Posch)

335) An Experimental Mixed Purpose Network (R.Posch, F.Pucher)

336) Detecting Cycles through Three Fixed Vertices in a Graph (H.Fleischner, G.Wöginger)

337) Scheduling with Incompatible Jobs (H.Bodlaender, K.Janse, G.Wöginger)

338) On-line Learning of Rectangle (Extended Abstract) (Z.Chen, W.Maass)

339) Helping the User to Select a Link (H.Maurer, I.Tomek)

340) Theory of Separability of Random Processes (R.Gudonavicius, G.Pfurtscheller)

341) The Architecture of a Massively Distributed Hypermedia System (F.Kappe, G.Pani)

342) A Process Synchronous CCD-Video Digitizer (H.Blattner, R.Posch)

343) Hypermedia Systems Without Links (H.Maurer, N.Scherbakov)

344) Trustworthy management of distribution and operation of encryption devices (R.Posch)

345) Fast Algorithms for the Maximum Convolution Problem (M.Bussieck, H.Hassler, G.Wöginger, T.Zimmermann)

346) Neural Network Based Classification of Simulated EEG Data: Sensitivity Analysis

347) Discovering Patterns in EEG-Signals: Comparative Study of Pattern Recognition and Machine Learning Methods (M.Kubat, D.Flotzinger, F.Pfurtscheller)

348) Multiagent Reasoning and Learning: General Framework (M.Kubat, S.Parsons)

349) Bounds for the Computational Power and Learning Complexity of Analog Neural Nets (W.Maass)

350) Electronical Committee Management (V.Ristic, P.Lipp, R.Posch)

351) EurIPACS/DECIS Expert Systems in Medicine (G.Gell)

352) GA-Driven Constructive Induction for Numeric-Data Analysis: Methodology and a Case Study (M.Kubat)

353) Towards Automated Sleep Classification in Infants Using Symbolic and Subsymbolic Approaches (M.Kubat, D.Flotzinger, G.Pfurtscheller)

354) Hypermedia Efforts and Hypermedia Philosophy at the Graz University of Technology (H.Maurer)

355) Interprocessor Communication in Distributed Transputer Systems (R.Ginthör, M.Platzner, R.Weiss)

356) Reasoning with Roughly Described Concepts (M.Kubat, S.Parsons)

357) Pipelining and full parallelism for long integer arithmetic in encryption devices (R.Posch)

358) Adaptive Identification of Ventricular beats and R-R-Interval Analysis in Noisy Long-term ECG Signals (H.Bakardjian, D.Gergen, G.Pfurtscheller)

359) Separating Paths in Infinite Planar Graphs (C.P.Bonnington, W.Imrich, M.E.Watkins)

360) A simple O(mn) algorithm for recognizing Hamming graphs (W.Imrich, S.Klavzar)

361) Hypermedia in Enterprises - A Critical Discussion (Ch.Schlögl)

362) Agnostic PAC-Learning of Functions on Analog Neural Nets (W.Maass)

363) From Hypertext to Active Communication/Information Systems (F.Kappe, H.Maurer)

364) Hyper-G: A Large Universal Hypermedia System and Some Spin-Offs (F.Kappe, H.Maurer)

365) On the Reconstruction of Cartesian-Product Graphs (W.Imrich, J.Zerovnik)

366) Neural Nets with Superlinear VC-Dimension (W.Maass)

367) Geodesics in Transitive Graphs (C.P.Bonnington, W.Imrich, N.Seifter)

368) Process and Product Measurement (V.Haase, G.Koch, R.Messnarz)

369) Feature Selection by Genetic Algorithms (D.Flotzinger)

370) Fast Identification of Geometric Objects with Membership Queries (W.J.Bultmann, W.Maass)

371) A Comparison of the Computational Power of Sigmoid and Boolean Threshold Circuits (W.Maass, G.Schnitger, E.D.Sontag)

372) On the Complexity of Function Learning (P.Auer, Ph.M.Long, W.Maass, G.J.Woeginger)

373) Skeletons, Recognition Algorithm and Distance Matrix of Quasi-Median Graphs (J.Hagauer)

374) Performance Measurement on a Multi-DSP Architecture with TMS320C40 (M.Platzner, Ch.Steger, R.Weiss)

375) MUSLI, A MUlti-Sensory Language Interface (J.Lennon, H.Maurer)

376) DynamIcons as Dynamic Graphic Interfaces: Interpreting the Meaning of a Visual Representation (D.H.Jonassen, R.Goldman-Segal, H.Maurer)

377) Multimedia Systems for the General Public: Experiences at World Expositions and Lessons Learned (H.Maurer, P.Sammer, A.Schneider)

378) Off-line Classification of EEG from the "New York Brain-Computer Interface (BCI)" (D.Flotzinger, J.Kalcher, J.R.Wolpaw, D.J.McFarland, G.Pfurtscheller)

379) Unique Keys Enabling Multithreshold Schemes (H.Hassler, R.Posch, V.Ristic)

380) Division in Residue Number Systems Involving Lenght Indicators (K.C.Posch, R.Posch)

381) High Performance Modular Arithmetic using an RNS based Chipset (J.Schwemmlein, R.Posch, K.C.Posch)

382) An Electronic Library and its Ramifications (H.Maurer, H.Mülner, A.Schneider)

383) Efficient Agnostic PAC-Learning with Simple Hypotheses (W.Maass)

384) Classifying Hyperplanes in Hypercubes (O.Aichholzer, F.Aurenhammer)

385) Perspectives of Current Research about the Complexity of Learning on Neural Nets (W.Maass)

386) From Personal Computer to Personal Assistant (J.Lennon, H.Maurer)

387) Levels of Anonymity (B.Flinn, H.Maurer)

388) Hyper-G: A New Tool for Distributed Hypermedia (F.Kappe, K.Andrews, J.Faschingbauer, M.Gaisbauer, M.Pichler, J.Schipflinger)

389) Advancing WWW: Hyper-G (H.Maurer)

390) On-line Learning with Malicious Noise and the Closure Algorithm (P.Auer, N.Cesa-Bianchi)

391) Autoregressive model based spectral analysis with application to EEG (G.Florian, G.Pfurtscheller)

392) Tree-Based Neural Net (TBNN) for Learning 'Difficult' Concepts (I.Ivanova, M.Kubat, G.Pfurtscheller)

393) On the Computational Complexity of Networks of Spiking Neurons (W.Maass)

394) Automated Feature Selection with a Distinction Sensitive Learning Vector *Quantizer*[1,2] (M.Pregenzer, G.Pfurtscheller, D.Flotzinger)

395) Efficient learning with virtual threshold gates (W.Maass, M.Warmuth)

396) Hypermedia Authoring with HM-Card (H.Maurer, N.Scherbakov, A.Schneider)

397) Computing the Maximum Bichromatic Discrepancy, with applications to Computer Graphics and Machine Learning (D.P.Dobkin, D.Gunopulos, W.Maass)

398) Lower Bounds for the Computational Power of Networks of Spiking Neurons (W.Maass)

399) Comparison of Different Light Reflection Models (K.F.Karner, E.A.Deutschl, F.W.Leberl)